Challenge Journal of Structural Mechanics

Research Article

Effect of different trimline extension of clear aligners in combination with Class II elastics on the mandibular dentition: a finite element analysis

Nurver Karslı [a,*], Bahanur Hilal Kisbet [a]

[a] *Department of Orthodontics, Karadeniz Technical University, 61080 Trabzon, Türkiye*

ABSTRACT

The objective of this study is to evaluate the effect of different trimline extension of aligners and the effect of elastics applied through the slit cutouts and buttons on the mandibular dentition using Class II intermaxillary elastics combined with clear aligner treatment. Three-dimensional (3D) finite element models that simulate the effects of Class II elastics on the mandibular arch in four different scenarios were studied, named, straight and high trimline aligner (HTLA) model with elastic applied through buttons (Model 1), straight and low trimline aligner (LTLA) model with elastic applied through buttons (Model 2), HTLA model with elastic applied through slit cutout (Model 3), LTLA model with elastic applied through slit cutout (Model 4). 3D displacements of the teeth, von Mises stress (VMS) in the periodontal ligament (PDL) were calculated. In all models, the crown of the mandibular anterior teeth moved labially, the root moved lingually, and the mandibular first molars moved mesially. Among all models, labialization of incisors and mesialization of molars was highest in Model 2 and lowest in Model 3. In clear aligner treatment combined with Class II elastics, HTLA was more effective in controlling mandibular incisor proclination and mesial tipping of mandibular molars. The slit cutout models were more effective in controlling mesial tipping of mandibular molars.

ARTICLE INFO

Article history:
Received 5 February 2024
Revised 14 March 2024
Accepted 10 April 2024

Keywords:
Clear aligner
Class II elastics
Incisor
Dentition
Finite element analysis

1. Introduction

Class II malocclusion is one of the most important reasons why patients seek orthodontic treatment and many different techniques can be preferred for its treatment; the use of intermaxillary elastics is one of these options as mentioned by Jones et al. (2008). In a recent study by Liu et al. (2022), intermaxillary elastics play an important role in the correction of many malocclusions, especially Class II malocclusions. Although CIIe has been demonstrated to provide beneficial effects, including anchorage support and the prevention of mesialization of maxillary posterior teeth, it has also been reported by Nelson et al. (2007) and Janson et al. (2013) that it can cause undesirable side effects, such as the proclination of mandibular anterior teeth. As stated by Patter-son et al. (2021), the use of ClIe in fixed orthodontic treatments inevitably results in loss of anchorage and reciprocal force transmission to the mandibular anterior teeth. This may cause side effects such as alveolar defects, fenestration and dehiscence, especially in patients with thin cortical bone in the lower anterior region, as reported by Evangelista et al. (2010). Therefore, to avoid these side effects, many researchers (Celikoglu et al 2016; Unal et al. 2015; Aslan et al. 2014; Luzi and Luzi 2013; Turkkahraman et al. 2016) have used various methods, such as utilizing skeletal anchorage devices and increasing the anchorage of the dental units involved.

In recent years, clear aligner treatment (CAT) has been preferred among patients seeking orthodontic treatment due to its ease and aesthetic features, and its treatment efficacy has increased with current develop-

* *Corresponding author*. E-mail address: nurverkarsli@ktu.edu.tr (N. Karslı)
ISSN: 2149-8024 / DOI: https://doi.org/10.20528/cjsmec.2024.02.003

ments, as reported in a study by Rossini et al. (2015). As Patterson et al. (2021) and Caruso et al. (2019) mentioned, CIIe can be applied from buttons adhered on the teeth or slit cutouts prepared on the aligner in CAT. According to Staderini et al. (2022), the side effects caused by CIIe, such as mandibular incisor proclination and posterior rotation of the palatal plane, can be compensated to some extent under clinical conditions because the aligners cover all teeth as a unit. However, further specific information is required on the study of the maxillary and mandibular dental arch in a force system that is complex.

The clinical results (Elkholy et al. 2019; Elshazly et al. 2022; Liu and Chen 2015) obtained in CAT are affected by many parameters such as the trimline extension of the aligner, the aligner material, the thickness of the aligner, the use of attachments, and the design of the attachment. Elhazy et al. (2022) found that high trimline aligner (HTLA) extending over the gingiva produced higher forces on the teeth. However, the trimming lines of ClearCorrect® aligners are designed to be straight and high, and this design has been scientifically proven to provide more accurate tooth movement and effective root control in a study by Elshazly et al. (2022). The study by Nicera et al. (2022) showed that the use of attachments increased the effectiveness of mesio-distal movements and that better anchorage of posterior teeth was obtained by increasing the number of attachments applied to the posterior teeth.

Finite element analysis (FEA) is a computational engineering method used to determine tooth displacements after the application of external forces. In recent years, FEA studies (Wang et al. 2022; Rossini et al. 2020) have been used in orthodontics to prove effective means of stimulating tooth movement patterns.

There is a lack of information in the literature regarding the effect of CAT with the use of CIIe, especially on the possible mandibular anterior teeth. Therefore, the aim of this current study was to evaluate the effects of different trimline extensions of the aligners and the application of elastic force through button or slit cutouts on the mandibular dentition in CAT combined with CIIe using FEA.

2. Materials and Methods

2.1. Model creation

The 3D mesh structure was arranged and mathematically transformed into a solid mesh structure. The generation of 3D FEA models and analysis were conducted on HP workstations equipped with INTEL Xeon E-2286 processors operating at a frequency of 2.40 GHz and 64 GB ECC memory.

The 3D Slicer Software was used to get the 3D model (.stl) of the bone structure using the CBCT data. The ANSYS SpaceClaim software was used for reverse engineering and 3D CAD activities. In addition, the adaptation of solid models to the analysis environment and optimized mesh creation activities were carried out with ANSYS Workbench software. LS-DYNA solver was used to solve the finite element models. The dimensions and cutout modifications of the aligner were based on the ClearCorrect® system.

2.2. Cortical bone, trabecular bone, teeth, and periodontal ligament

Pre-existing CBCT data from an adult patient with Class II malocclusion with complete dentition was used to obtain the bone model used in this study. The thickness of every CBCT slice was adjusted to 0.10 mm. The CBCT data, formatted as DICOM, was partitioned based on suitable Hounsfield values using the 3DSlider program. Subsequently, the data was transformed into a three-dimensional model by segmentation. The threshold procedure was used to create mask layers of maxillary and mandibular bone, tooth structure, mandible and temporomandibular joint (TMJ).

The 3D model was imported into the ANSYS SpaceClaim software, where the maxillary and mandibular cortical bone and tooth geometry were modeled. The trabecular bone has been obtained by reference the inside of the 3D mandibular cortical bone. The disc was modeled using an anatomic structure. A periodontal ligament model with a thickness of 0.25 mm was created using the outer surface of the dentin model. All the prepared models were placed in the correct coordinates in 3D space in ANSYS SpaceClaim software and the modeling process was completed (Fig. 1). Vertical rectangular attachments (2×3×1 mm) on the buccal surface of the lower canine and premolar teeth were added for retention.

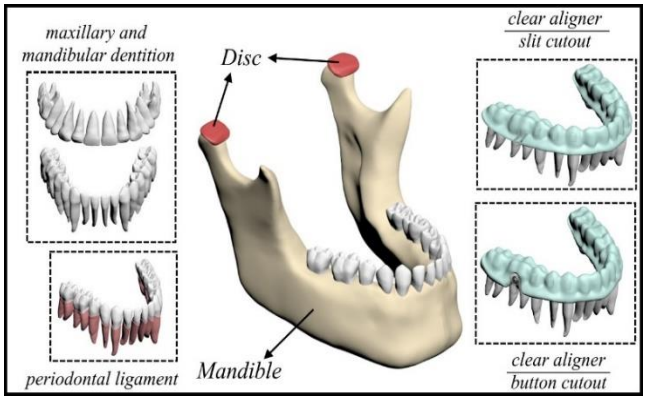

Fig. 1. Different components of the model.

2.3. Creating analysis models from the original 3D model

The button used in this study was modeled in ANSYS SpaceClaim software. Two main models as button and slit cutout were designed. Each of the main models were designed to the 0.76 mm thick aligners as HTLA (straight and high trimline that extends 2 mm above the gingival margin) and LTLA (straight and low trimline that extends 0.5 mm above the gingival margin). Thus, four different models were prepared for analysis (Fig. 2). The modifications of the prepared models are given in Table 1.

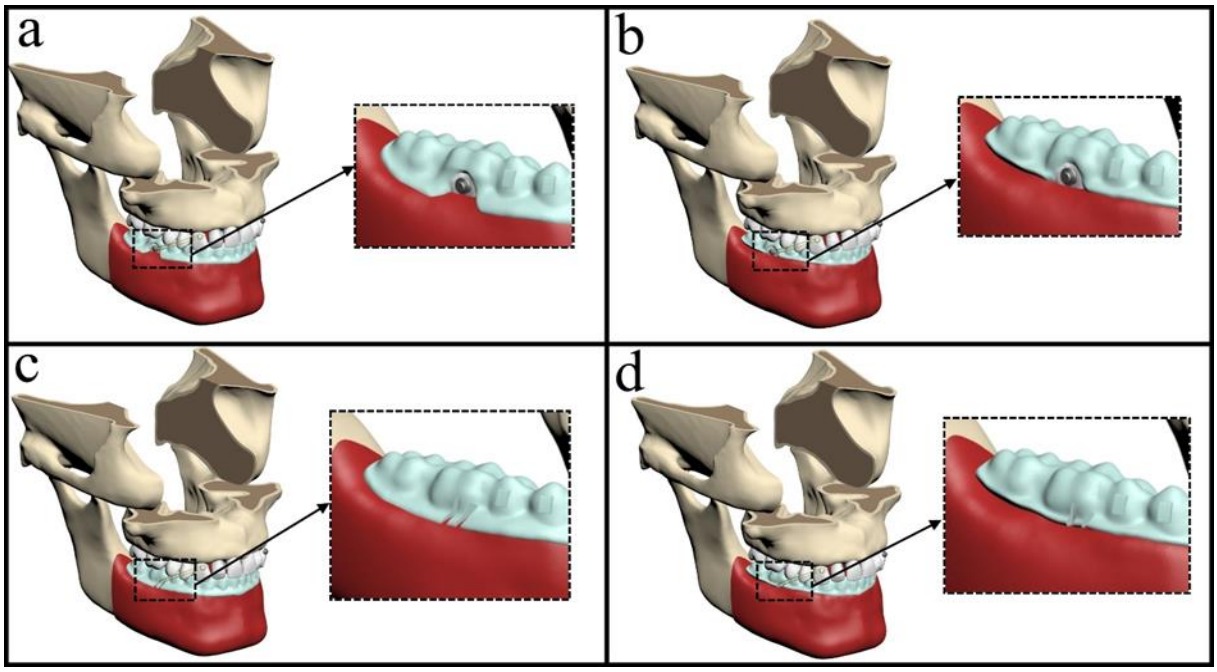

Fig. 2. Finite element models:
(a) Model 1 (straight and high trimline aligner (HTLA) model with elastic applied through button);
(b) Model 2 (straight and low trimline aligner (LTLA) model with elastic applied through button;
(c) Model 3 (HTLA model with elastic applied through slit cutout);
(d) Model 4 (LTLA model with elastic applied through slit cutout).
The black square areas represent close-up views the aligner cutout and the aligner trimline extension.

Table 1. Modifications of the models.

Models	Trimline extension	Aligner cutouts
Model 1	High	Button
Model 2	Low	Button
Model 3	High	Slit
Model 4	Low	Slit

2.4. Obtaining mathematical models

Mathematical models were created by partitioning geometric models into discrete and compact parts referred to as meshes. The modeling procedure was conducted using ANSYS SpaceClaim software, while the models were generated mathematically using ANSYS Workbench software. Subsequently, the models were prepared for analysis. The mathematical models created in ANSYS Workbench software were transferred to the LS-DYNA solver for analysis.

2.5. Material properties

The material properties of the investigated model are quantitatively specified in Table 2. The examinations used linear material properties, including the elastic modulus and Poisson's ratio.

Table 2. Linear material properties.

Material	Elastic modulus (MPa)	Poisson's ratio (ν)
Cortical Bone (Liu et al. 2022; Chen et al. 2019)	1.37×10^4	0.26
Trabecular Bone (Liu et al. 2022; Chen et al. 2019)	1.37×10^3	0.30
Tooth (Liu et al. 2022, 2023)	1.96×10^4	0.30
PDL (de Oliveira et al. 2020; Li et al. 2006)	6.9×10^{-1}	0.45
Mucosa (Hohmann et al. 2007)	2.8	0.40
Button (Liu et al. 2023; Ammar et al. 2011)	1.14×10^5	0.35
CA (Liu et al. 2022, 2023)	5.28×10^2	0.36
Attachments (Liu et al. 2022, 2023)	1.25×10^4	0.36
Condylar cartilage (Liu et al. 2022, 2023)	8×10^{-1}	0.30
Disc (Liu et al. 2022, 2023)	1.8×10^{-1}	0.40

***PDL, periodontal ligament; CA, clear aligner.

2.6. Loading and boundary conditions

A force of 120 g (~1.177 N) was applied to maxillary canines and mandibular first molars by CIIe.

In the slit cutout models; a total force of 120 g was applied from the slit cutout on the aligner to the button on the maxillary canine. In button cutout models; a load representing 120 g of force was applied from the button on the maxillary canine to the button on the mandibular first molar.

The models were bound at the nodal points in the upper part of the maxillary bones, thereby constraining all degrees of freedom to prohibit any movement in the three axes. A total of six nonlinear static analyses were conducted on six analysis models, with the force and boundary conditions indicated. Based on the boundary criteria, the lower border of the mandible is immobilized and the upper region is restricted the movement of the maxillary and temporal structures. The attachment contact was set at the interfaces from cancellous bone to cortical bone, cortical bone to PDL, PDL to tooth and tooth to attachment. This bonding prevented any movement between the contact surfaces. Furthermore, the joints between the teeth were not separated at their interfaces, allowing some frictionless sliding along the contact surfaces. In order to be able to apply the analysis in the mathematical models created and to obtain accurate results, the surface relations between the parts must be defined in the analysis program.

A nonlinear frictional contact with a coefficient $\mu = 0.2$ was set at the aligner-tooth and aligner-attachment interfaces. The tooth-PDL, tooth-attachment, and cortical and trabecular bone-PDL contact areas were designated as bonded-type contact. This approach is based on the assumption that the parts move with full correlation during their movement. The mesh structure and boundary condition of model were shown in Fig. 3.

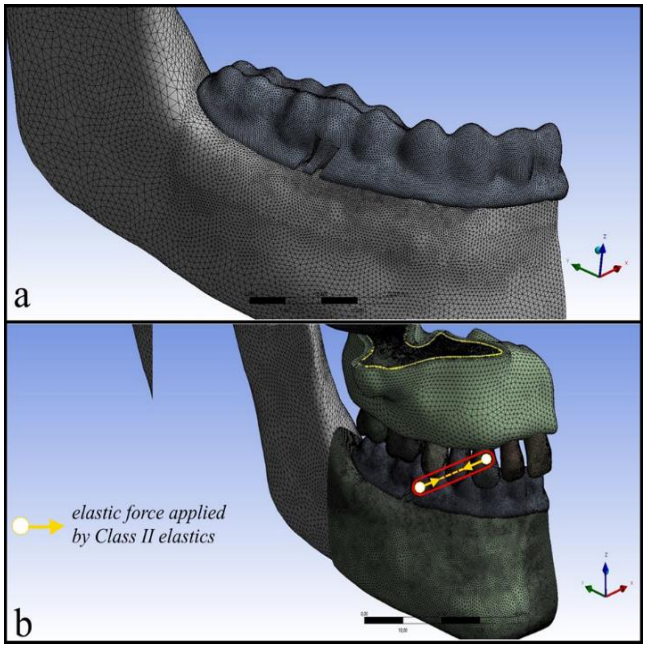

Fig. 3. (a) Mesh structure; (b) Global coordinate and boundary condition of model.

2.7. Outcomes

The global coordinate system shown in Fig. 3 was created for the mandibular tooth structure. In this system, the *x*-axis relates to the coronal plane, with positive values indicating the left side and negative values indicating the right side. The *y*-axis indicates the sagittal plane, with positive values indicating the posterior direction and negative values indicating the anterior direction. Lastly, the *z*-axis indicates the vertical plane, with positive values indicating the superior direction and negative values indicating the inferior direction. Each tooth was assigned a local coordination system, with the *x*-axis indicating the mesial direction (+) and the distal direction (-), the *y*-axis indicating the lingual direction (+) and the buccal direction (-), and the positive direction on the *z*-axis being indicated by the apex of the mandibular teeth and the incisor/occlusal of the mandibular teeth.

2.8. Quantitative model information

The mesh properties created in the prepared analysis models are given in Table 3. In all models, mesh quality was checked for the triangles that have skewness > 80°, and minimum length of 0.001. Failed meshes were edited accordingly.

Table 3. Nodes and elements.

Models	Nodes	Elements
Model 1	415551	1528465
Model 2	422270	1553124
Model 3	412867	1517856
Model 4	419153	1540841

3. Results

3.1. Aligner deformation

During the mesialization of the mandibular arch with CIIe force, different behaviors and force systems were recorded among the simulations performed. Data for maximum and minimum aligner deformation are given in Appendix A and Figs. 4(a-d). The maximum aligner deformation among the models was observed in Model 3 (slit cutout-high) in the region of the slit cutout of the first molar (0.0817 mm). The maximum aligner deformation was concentrated on the buccal slit cutout region of the first molars in Models 3 and 4, on the mesiobuccal cusp region of the first molars in Models 1 and 2, while the minimum aligner deformation was observed on the bucco-gingival region of the canine teeth in all models.

3.2. Three-dimensional movement of the mandibular dentition

The displacement of the teeth has been recorded according on the global coordinate system. The movement of the mandibular dentition occurred mostly in the sag-

ittal plane toward the *y*-axis. The mandibular dentition of all models moved forward with extrusion tendency of molars and intrusion of anterior teeth due to the CIIe force (Figs. 5(a-d) and Appendix B).

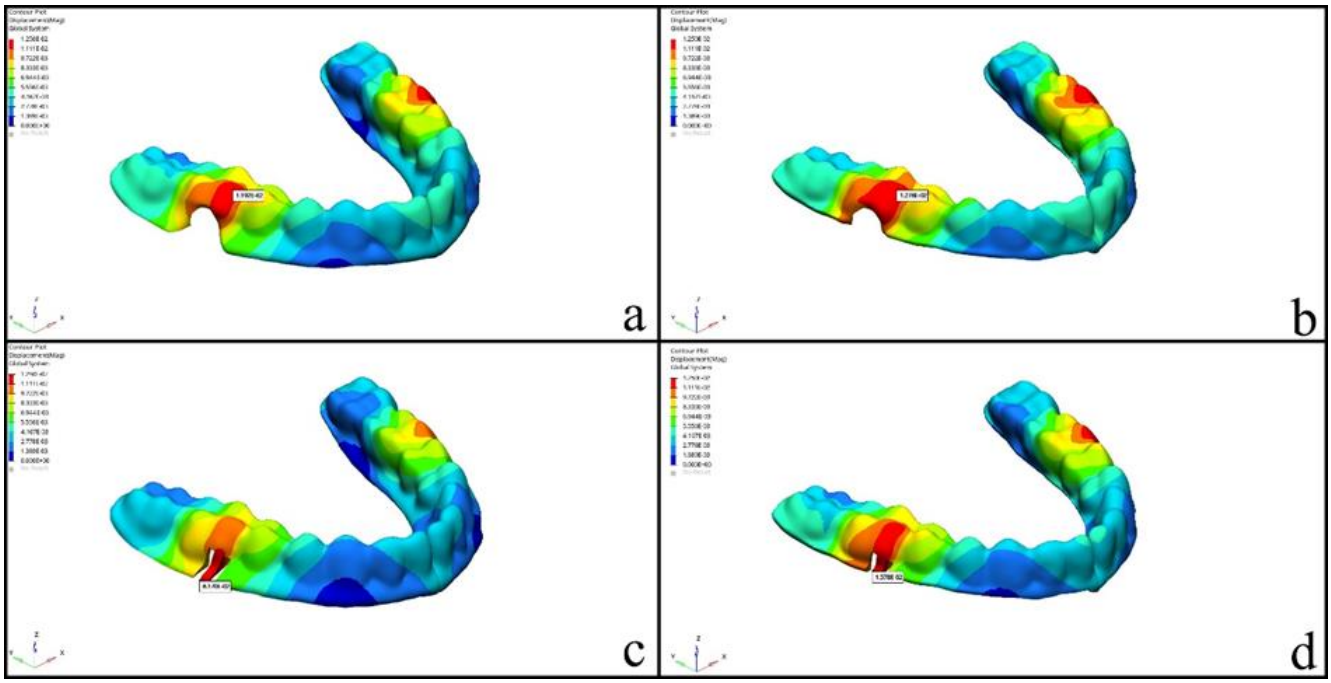

Fig. 4. Clear aligner deformation values:
(a) Model 1 (straight and high trimline aligner (HTLA) model with elastic applied through button);
(b) Model 2 (straight and low trimline aligner (LTLA) model with elastic applied through button);
(c) Model 3 (HTLA model with elastic applied through slit cutout);
(d) Model 4 (LTLA model with elastic applied through slit cutout).

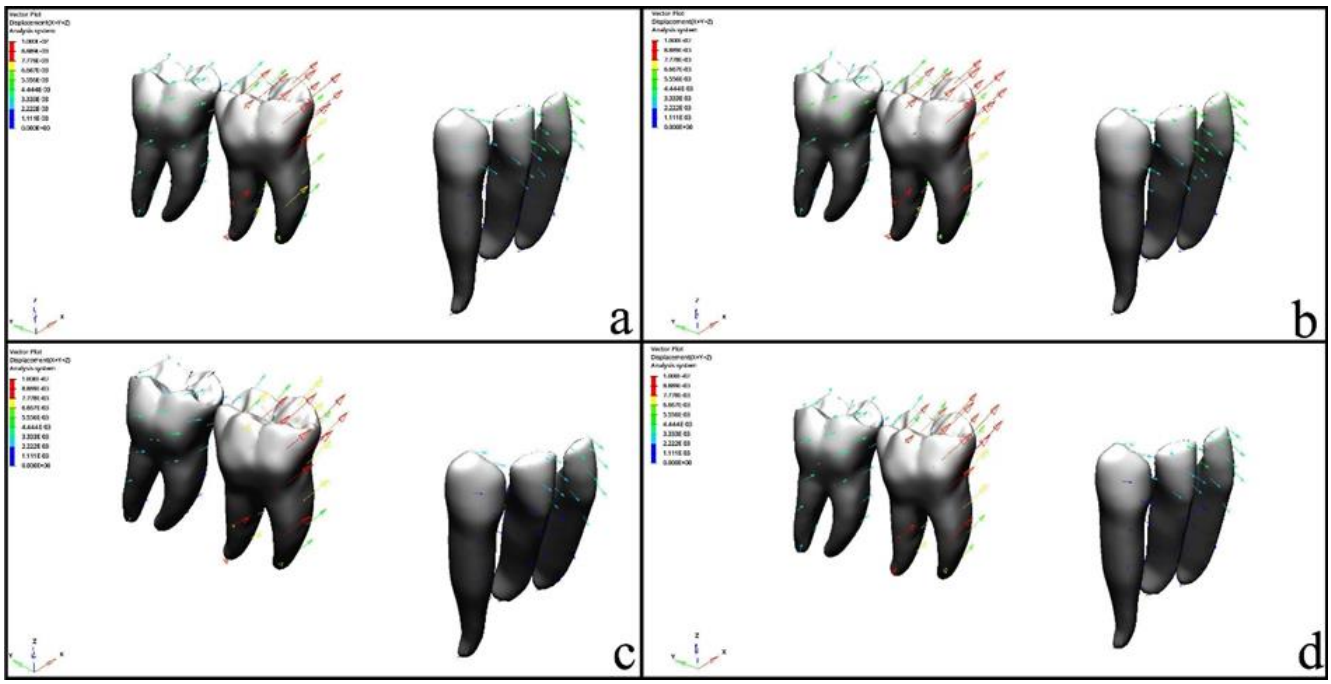

Fig. 5. The directional inclination of the lower teeth in models that received Class II elastics:
(a) Model 1 (straight and high trimline aligner (HTLA) model with elastic applied through button);
(b) Model 2 (straight and low trimline aligner (LTLA) model with elastic applied through button;
(c) Model 3 (HTLA model with elastic applied through slit cutout);
(d) Model 4 (LTLA model with elastic applied through slit cutout).

3.3. Three-dimensional displacement of mandibular anterior teeth

The 3D displacements of the mandibular anterior teeth in all models are shown in Appendix B and Figs. 6(a-d).

Mandibular central and lateral incisors;

In the mesio-distal direction (*x*-axis), the crown exhibited mesial movement and the root exhibited distal movement in all models. Among all models, the highest movement was observed in Models 1 and 2 (L1, 0.0010; L2, 0.0012 mm), and the least movement was observed in Model 4 (L1, 0.0007; L2, 0.0010 mm).

In the labio-lingual direction (*y*-axis), the crown exhibited buccal movement and the root exhibited lingual movement in all models. Among all models, the greatest labial crown movement was observed in Model 2 (L1, 0.0044; L2, 0.0039 mm), and the least labial movement was observed in Model 3 (L1, 0.0032; L2, 0.0027 mm).

In the supero-inferior direction (*z*-axis), the crown and root moved inferiorly (intrusion) in all groups. Among all groups, the highest inferior movement was observed in Model 4 (L1, 0.0025; L2, 0.0018 mm), and the least in Model 3 (L1, 0.0017; L2, 0.0011 mm).

Mandibular canines;

In the *x*-axis, the crown moved mesially and the root moved distally in all models. Among all models, the maximum mesial movement of the crown was observed in Model 2, (0.0025 mm), and the minimum mesial movement was observed in Model 3 (0.0020 mm).

In the *y*-axis, the crown moved buccally and the root moved lingually in all models. Among all models, the most labial crown movement was observed in Model 2 (0.0029 mm), and the least buccal crown movement was observed in Model 3 (0.0019 mm).

In the *z*-axis, the crown and root moved inferiorly in all models. Among all models, the most inferior movement was observed in Model 2 (0.0007 mm), while the least inferior movement was observed in Model 3 (0.0003 mm).

3.4. Three-dimensional displacement of mandibular molars

The 3D displacements of the mandibular molars in all models are shown in Appendix B and Figs. 6(a-d).

Mandibular first molars;

In the bucco-lingual direction (*x*-axis), lingual tipping with mesiolingual rotation was observed in all models. Among all models, the highest amount of lingual tipping with rotation was observed in Model 2 (0.0100 mm) and, the least in Model 3 (0.0083 mm).

In the mesio-distal direction (*y*-axis), mesial displacement was observed in all models. The greatest mesial displacement was observed in Model 2 (0.0042 mm), followed by Model 1 and Model 4, respectively. The least mesial displacement was found in Model 3 (0.0028).

In the supero-inferior direction (*z*-axis), the crown and root moved superiorly (extrusion) in all models. Among all models, the highest extrusion movement was observed in Model 4 (0.0052 mm), and the least in Model 3 (0.0015 mm).

Mandibular second molars;

In the *x*-axis, lingual tipping with mesiolingual rotation was observed in all models. The highest amount of lingual tipping with rotation was observed in Model 2 (0.0016 mm), and the lowest in Model 3 (0.0010 mm).

In the *y*-axis, the crown and root moved mesially in all models, with a higher displacement in the crown. The highest mesial displacement was observed in Model 2 (0.0037 mm), and the lowest in Model 3 (0.0029 mm).

In the z*x*-axis, the crown and root were displaced superiorly (extrusion) in all models. Among all models, the highest extrusion movement was observed in Model 2 (0.0029 mm) and the lowest in Model 3 (0.0019 mm).

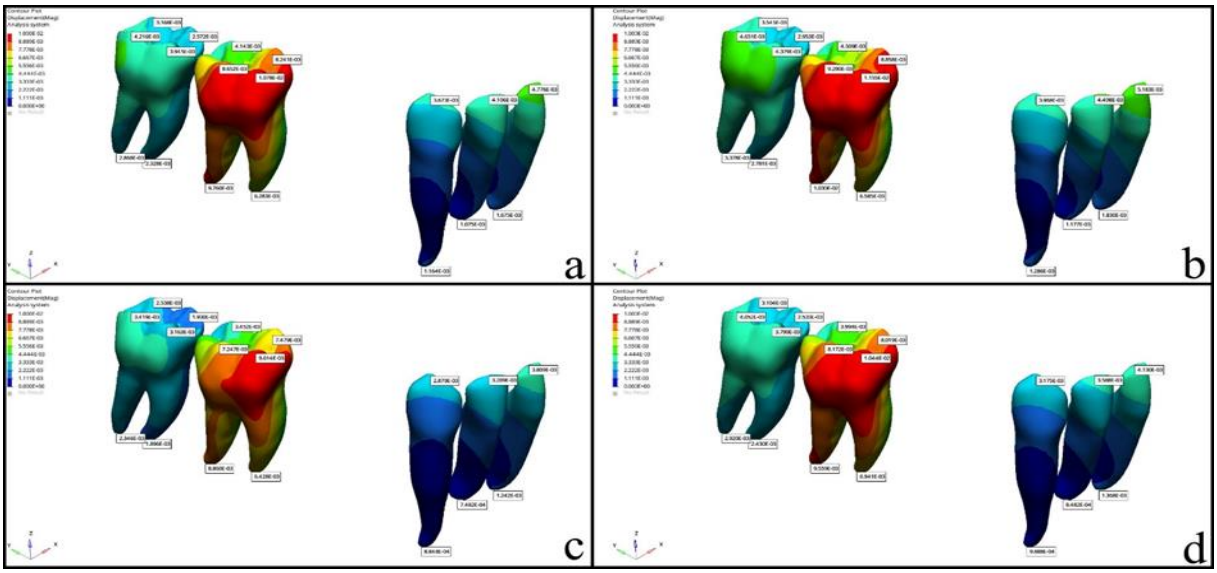

Fig. 6. A propensity for three-dimensional displacement of the mandibular dentition in Class II elastic models:
(a) Model 1 (straight and high trimline aligner (HTLA) model with elastic applied through button);
(b) Model 2 (straight and low trimline aligner (LTLA) model with elastic applied through button;
(c) Model 3 (HTLA model with elastic applied through slit cutout);
(d) Model 4 (LTLA model with elastic applied through slit cutout).

3.5. Stress distribution

The stress distribution values and regions occurring in the PDL are presented in Appendix C and Figs. 7(a-d).

In all models, maximum stress values were observed at the buccal root of the maxillary first molars and the highest PDL stress was found in Model 4 (0.0150 MPa).

The highest PDL stress was concentrated in the labial and cervical region of the incisors, and the highest stress was found in Model 2 (L1, 0.0046 MPa; L2, 0.0040 MPa) among all models.

The maximum PDL stress was found to be concentrated in the lingual and cervical region of the canines, and the highest stress was observed in Model 2 (0.0038 MPa) among all models.

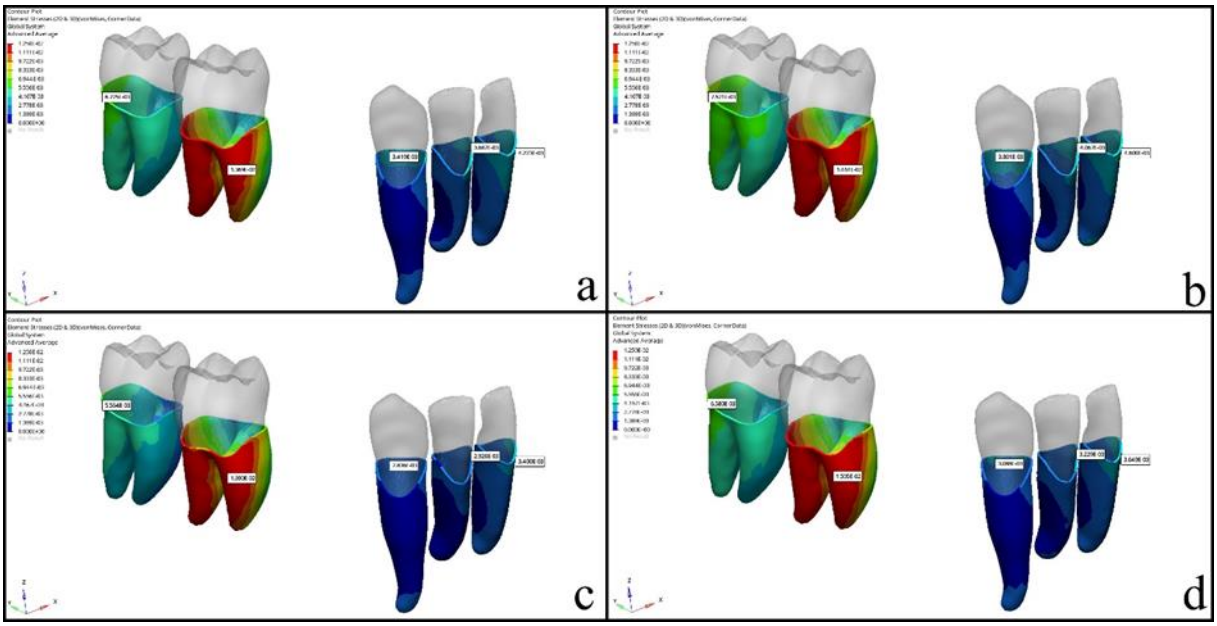

Fig. 7. The stress distribution of PDL:
(a) Model 1 (straight and high trimline aligner (HTLA) model with elastic applied through button);
(b) Model 2 (straight and low trimline aligner (LTLA) model with elastic applied through button;
(c) Model 3 (HTLA model with elastic applied through slit cutout);
(d) Model 4 (LTLA model with elastic applied through slit cutout).

4. Discussion

The popularity of CAT has been increasing due to its significant advantages, including cosmetic and comfort benefits. Along with the developing aligner industry, different aligner designs are also gaining attention in the industry, and one of these variables is the trimline extension of the aligners. Previous experimental studies (Elshazly et al. 2022; Cowley 2012; Brown 2021; Gao and Wichelhaus 2017) have also reported the importance of the trimline design and extension of aligners for orthodontic treatment planning.

In aligner therapy of some complex cases, additional mechanics such as ClIe may be required for additional anchorage. At this point, the factor of where to apply the intermaxillary elastics comes to the fore; the elastics can be applied through the precision cutouts designed on the aligner or through the buttons added on the teeth. Liu et al. (2022) also reported that CIIe applied through slit cutouts transfers the force directly through the aligner and elastic force applied through buttons transfers the force directly to the tooth where the button is applied and then spreads it to the other teeth. In addition, intermaxillary elastics combined with CAT can effectively correct the sagittal relationship and have many positive contributions in terms of anchorage and treatment time. However, the number of studies investigating the effects of CAT combined with CIIe on the mandibular dentition is quite limited. In the light of all this information, our study investigates the effects of the area of application of the elastics and the trimline extension of the aligners on the mandibular arch in CAT combined with CIIe.

FEA is a mathematical method that can precisely evaluate the changes in complex geometric shapes and the stresses and strains that occur on them, which is frequently used in orthodontics. Studies in the literature (Kucukkurt 2019; Knop et al. 2015) have also indicated that FEA is an effective method for precisely measuring changes in teeth and VMS.

In previous research conducted by Liu et al. (2023), it was demonstrated that correcting the molar relationship using CIIe combined with CAT involved moving the maxillary molars posterior and the mandibular molars forward. In our study, mesialization was observed in mandibular molar teeth with the effect of the force applied with CIIe. The force vector of CIIe applied through the button on the buccal side of the mandibular molar or through the slit cutouts on the aligner can be divided into lingual and superior components, with the mesial force being greater in the study by Liu et al. (2022). Therefore,

lingual tipping with mesio-lingual rotation was observed in mandibular molars in this study. Liu et al. (2022) found that CIIe applied through the button provided more effective molar mesialization than those applied through the slit cutout. They attributed this to the fact that mandibular molar mesialization was greater with the force applied directly to the tooth from the button. Furthermore, the results obtained in the present study are consistent with these findings. It was seen that models with slit cutout and high trimline extension provided more control over mesial tipping and rotation during mesial movement of the first molars. The improved control of tooth movement observed in the high trimline and slit cutout models can be attributed to the optimization of forces resulting from the expanded surface area over which the force is transmitted by the high trimline aligners, as well as the utilization of elastics through the slit cuts to ensure that the force is not directly applied to the tooth, thereby optimizing force distribution. Moreover, the increased mesial rotation observed in the button models can be attributed to the presence of a gap between the aligners and teeth. This gap is further exacerbated when the aligner fit is inadequate particularly in patients where the aligners are not tracking properly. Hence, this gap would prevent the aligner to overcome the mesial rotation effect of Clle, when applied through a button. It can be proposed that greater control over overturning in the slit-cutout and high trimline model can be attributed to the fact that the force applied by the CIIe is directed towards the centre of resistance of the tooth.

Previous studies (Nelson et al. 2005; Janson et al. 2013) have shown that the use of CIIe causes some side effects such as undesirable proclination of the mandibular anterior teeth. In our study, labial tipping of the mandibular incisors was observed to varying degrees in all models and it was found that labial tipping of the mandibular incisors was higher in models with a low trimline extension. This information allows us to interpret that incisor proclination may be more controllable in treatment with aligners with a high trimline extension. In addition, Liu et al. (2022) reported that additional optimized torque designs can be planned for the control of the proclination of the mandibular anterior teeth.

The proclination of the mandibular anterior teeth leads to the concentration of strains on the periodontal ligament (PDL) and alveolar bone in the cervical region of the labial surface. Some investigators reported an increased risk of root resorption due to the pressure on the PDL exceeding the capillary pressure in the area and impaired blood flow. Furthermore, previous studies (Hohmann et al. 2007; Dorow and Sander 2005) showed that the PDL pressure threshold involved in root resorption is 0.047 MPa. Although none of the models exceeded this threshold for PDL stress, this threshold was relatively close, especially in the low LTLA and button cutout model (0.0046 MPA). This may be attributed to the fact that low trimline extension aligners are less effective in controlling the proclination of mandibular anterior teeth. Moreover, PDL stress values were measured to be lower in slit cutout models than in button models.

Although FEA is a widely used technology for biomechanical analysis of applied forces in orthodontics, it is inevitable to say that it has some limitations. Although it is possible to optimally adjust the magnitude and vector of the applied force initially, the direction and intensity of the force are constantly changing with tooth movement during clinical practice. Furthermore, these models cannot take into account complex masticatory pressures and bone remodeling. On the other hand, in this FEA study (Tanne et al. 1987), the PDL thickness was assumed to be constant; however, the PDL varies in thickness along the tooth root. In their study, Hohmann et al. (2011) suggested that this nonlinear change in PDL thickness changes the elastic modulus of the PDL, which in turn affects the VMS values. Therefore, clinical studies evaluating the effects of CIIe applied with aligners on mandibular anterior teeth are needed and future studies should investigate the dynamic behavior of the dentition when using CAT in combination with CIIe.

In terms of the clinical importance of these findings, it can be stated that utilizing a Clle with buttons is a preferable option for patients with short crowns. However, it does have the drawbacks of inducing tipping and mesial rotation. Hence, it might be imperative to incorporate anti-rotation movement to the lower molars in patients who would necessitate prolonged use of Clle.

5. Conclusions

Clear aligners with high trimline extension were found to be more effective in controlling lower anterior teeth. Less mesial movement was observed in mandibular molars due to increased aligner deformation by ClIe applied through slit cutouts. The presence of high trimline aligners and the application of CIIe from the slit cutout were found to increase the control of mesial tipping of mandibular molars.

Appendix A. Aligner deformation and location

Aligner deformation	Maximum deformation (mm)	Localization	Minimum deformation (mm)	Localization
Model 1	0.0119	Mesio-buccal cusp of mandibular first molar	0	Bucco-gingival edges of canine
Model 2	0.0127	Mesio-buccal cusp of mandibular first molar	0.0013	Bucco-gingival edges of canine
Model 3	0.0817	Slit cutout region of mandibular first molar	0	Bucco-gingival edges of canine
Model 4	0.0157	Slit cutout region of mandibular first molar	0	Bucco-gingival edges of canine

Appendix B. Three-dimensional displacement of mandibular teeth

Tooth	Axes	*x*-axis				*y*-axis				*z*-axis			
	Models	1	2	3	4	1	2	3	4	1	2	3	4
Central incisor	C	0.0010	0.0010	0.0008	0.0007	-0.0040	-0.0044	-0.0032	-0.0036	-0.0023	-0.0025	-0.0017	-0.0018
	R	-0.0003	-0.0003	-0.0002	-0.0002	0.0014	0.0015	0.0010	0.0012	-0.0008	-0.0008	-0.0005	-0.0005
Lateral incisor	C	0.0012	0.0012	0.0010	0.0010	-0.0035	-0.0039	-0.0027	-0.0031	-0.0016	-0.0018	-0.0011	-0.0013
	R	-0.0003	-0.0003	-0.0025	-0.0002	0.0008	0.0009	0.0006	0.0007	-0.0005	-0.0005	-0.0002	-0.0003
Canine	C	0.0024	0.0025	0.0020	0.0020	-0.0026	-0.0029	-0.0019	-0.0024	-0.0006	-0.0007	-0.0003	-0.0003
	R	-0.0007	-0.0007	-0.0006	-0.0006	0.0008	0.0009	0.0005	0.0007	-0.0003	-0.0003	-0.0000	-0.0001
First molar	CMB	0.0093	0.0100	0.0083	0.0088	-0.0032	-0.0033	-0.0020	-0.0025	0.0042	0.0046	0.0043	0.0049
	CML	0.0080	0.0086	0.0071	0.0076	-0.0003	-0.0003	0.0005	0.0001	0.0016	0.0018	0.0020	0.0025
	CDB	0.0059	0.0063	0.0051	0.0054	-0.0040	-0.0042	-0.0028	-0.0034	0.0048	0.0052	0.0042	0.0049
	CDL	0.0035	0.0038	0.0030	0.0033	-0.0007	-0.0007	0.0000	-0.0003	0.0019	0.0021	0.0015	0.0022
	AM	-0.0031	-0.0031	-0.0020	-0.0022	-0.0033	-0.0033	-0.0042	-0.0043	0.0043	0.0046	0.0043	0.0049
	AD	-0.0065	-0.0068	-0.0051	-0.0054	-0.0048	-0.0049	-0.0056	-0.0057	0.0053	0.0058	0.0044	0.0053
Second molar	CMB	0.0013	0.0016	0.0010	0.0013	-0.0033	-0.0035	-0.0027	-0.0031	0.0015	0.0019	0.0011	0.0016
	CML	0.0009	0.0011	0.0007	0.0009	-0.0016	-0.0017	-0.0011	-0.0014	0.0017	0.0021	0.0013	0.0018
	CDB	-0.0003	-0.0003	-0.0005	-0.0003	-0.0035	-0.0037	-0.0029	-0.0033	0.0022	0.0026	0.0017	0.0023
	CDL	-0.0009	-0.0008	-0.0010	-0.0008	-0.0016	-0.0017	-0.0012	-0.0014	0.0025	0.0029	0.0019	0.0025
	AM	0.0003	0.0003	0.0002	0.0003	-0.0011	-0.0013	-0.0010	-0.0012	0.0019	0.0024	0.0015	0.0020
	AD	-0.0006	-0.0007	-0.0006	-0.0006	-0.0013	-0.0015	-0.0012	-0.0013	0.0024	0.0029	0.0018	0.0024

C, crown; R, root; CMB, mesiobuccal cusp; CML, mesiolingual cusp; CDB, distobuccal cusp;
CDL, distolingual cusp; AM, Mesial root apex; AD, distal root apex.

Appendix C. von Mises stress values and distribution in the mandibular dentition

Models	PDL stress	Maximum value (MPa)	Localization	Minimum value (MPa)	Localization
Model 1	Central Incisor	0.0042	Bucco-gingival root surface	0	Disto-apical root surface
	Lateral Incisor	0.0036	Bucco-gingival root surface	0	Disto-lingual root surface
	Canine	0.0034	Linguo-gingival root surface	0	Buccal root surface
	First Molar	0.0136	Buccal root surface	0.001	Cervico-lingual root surface
	Second Molar	0.0067	Disto-gingival root surface	0.001	Mesio-lingual root surface
Model 2	Central Incisor	0.0046	Bucco-gingival root surface	0	Disto-apical root surface
	Lateral Incisor	0.0040	Bucco-gingival root surface	0	Disto-lingual root surface
	Canine	0.0038	Linguo-gingival root surface	0	Buccal root surface
	First Molar	0.0146	Buccal root surface	0.001	Cervico-lingual root surface
	Second Molar	0.0075	Disto-gingival root surface	0.001	Mesio-lingual root surface
Model 3	Central Incisor	0.0034	Bucco-gingival root surface	0	Disto-apical root surface
	Lateral Incisor	0.0029	Bucco-gingival root surface	0	Disto-lingual root surface
	Canine	0.0028	Linguo-gingival root surface	0	Buccal root surface
	First Molar	0.0139	Buccal root surface	0	Cervico-lingual root surface
	Second Molar	0.0055	Disto-gingival root surface	0	Mesio-lingual root surface
Model 4	Central Incisor	0.0036	Bucco-gingival root surface	0	Disto-apical root surface
	Lateral Incisor	0.0032	Bucco-gingival root surface	0	Disto-lingual root surface
	Canine	0.0030	Linguo-gingival root surface	0	Buccal root surface
	First Molar	0.0150	Buccal root surface	0.001	Cervico-lingual root surface
	Second Molar	0.0065	Disto-gingival root surface	0.001	Mesio-lingual root surface

Acknowledgements

The authors would like to thank Tinus Technologies, ClearCorrect and its employees for their technical contributions, and Dr. Arda Dilgiloğlu and Assoc. Prof. Dr. Hüccet Kahramanzade for sharing their knowledge and experience.

Funding

The authors received no financial support for the research, authorship, and/or publication of this manuscript.

Conflict of Interest

The authors declared no potential conflicts of interest with respect to the research, authorship, and/or publication of this manuscript.

Author Contributions

All of the authors made substantial contributions to conception and design, or acquisition of data, or analysis and interpretation of data; were involved in drafting the manuscript or revising it critically for important intellectual content; and gave final approval of the version to be published.

Data Availability

The datasets created and/or analyzed during the current study are not publicly available, but are available from the corresponding author upon reasonable request.

REFERENCES

Ammar HH, Ngan P, Crout RJ, Mucino VH, Mukdadi OM (2011). Three-dimensional modeling and finite element analysis in treatment planning for orthodontic tooth movement. *American Journal of Orthodontics and Dentofacial Orthopedics*, 139(1), e59–71.

Aslan BI, Kucukkaraca E, Turkoz C, Dincer M (2014). Treatment effects of the Forsus Fatigue Resistant Device used with miniscrew anchorage. *The Angle Orthodontist*, 84(1), 76-87.

Brown BE (2021). Effect of Gingival Margin Design on Clear Aligner Material Strain and Force Delivery. Thesis. University of Minnesota.

Caruso S, Nota A, Ehsani S, Maddalone E, Ojima K, Tecco S (2019). Impact of molar teeth distalization with clear aligners on occlusal vertical dimension: a retrospective study. *BMC Oral Health*, 19(1), 182.

Celikoglu M, Buyuk SK, Ekizer A, Unal T (2016). Treatment effects of skeletally anchored Forsus FRD EZ and Herbst appliances: A retrospective clinical study. *The Angle Orthodontist*, 86(2), 306-314.

Chen X, Mao B, Zhu Z, Yu J, Lu Y, Zhang Q, Yue L, Yu H (2019). A three-dimensional finite element analysis of mechanical function for 4 removable partial denture designs with 3 framework materials: CoCr, Ti-6Al-4V alloy and PEEK. *Scientific Reports*, 9(1), 13975.

Cowley DP (2012). Effect of Gingival Margin Design on Retention of Thermoformed Orthodontic Aligners. Thesis. University of Nevada.

de Oliveira JC, Sordi MB, da Cruz ACC, Zanetti RV, Betiol EAG, Vieira SR, Zanetti AL (2020). Number of dental abutments influencing the biomechanical behavior of tooth–implant-supported fixed partial dentures: A finite element analysis. *Journal of Dental Research, Dental Clinics, Dental Prospects*, 14(4), 228-234.

Dorow C, Sander FG (2005). Development of a model for the simulation of orthodontic load on lower first premolars using the finite element method. *Journal of Orofacial Orthopedics / Fortschritte der Kieferorthopädie*, 66(3), 208-218.

Elkholy F, Mikhaiel B, Repky S, Schmidt F, Lapatki BG (2019). Effect of different attachment geometries on the mechanical load exerted by PET G aligners during derotation of mandibular canines. J*ournal of Orofacial Orthopedics / Fortschritte der Kieferorthopädie*, 80(6), 315-326.

Elshazly T, Salvatori D, Bourauel C, Elattar H, Alkabani Y. (2022). Effect of thickness and material type of orthodontic aligners on force transmission: An in vitro study using pressure-sensitive films. *SSRN*, 4270102.

Elshazly TM, Keilig L, Salvatori D, Chavanne P, Aldesoki M, Bourauel C (2022). Effect of trimming line design and edge extension of orthodontic aligners on force transmission: An in vitro study. *Journal of Dentistry*, 125, 104276.

Evangelista K, Vasconcelos K de F, Bumann A, Hirsch E, Nitka M, Silva MAG (2010). Dehiscence and fenestration in patients with Class I and Class II Division 1 malocclusion assessed with cone-beam computed tomography. *American Journal of Orthodontics and Dentofacial Orthopedics*, 138(2), 133.e1-133.e7.

Gao L, Wichelhaus A (2017). Forces and moments delivered by the PET-G aligner to a maxillary central incisor for palatal tipping and intrusion. *The Angle Orthodontist*, 87(4), 534-541.

Hohmann A, Kober C, Young P, Dorow C, Geiger M, Boryor A, Sander FM, Sander C, Sander FG (2011). Influence of different modeling strategies for the periodontal ligament on finite element simulation results. *American Journal of Orthodontics and Dentofacial Orthopedics*, 139(6), 775-783.

Hohmann A, Wolfram U, Geiger M, Boryor A, Sander C, Faltin R, Faltin K, Sander FG (2007). Periodontal ligament hydrostatic pressure with areas of root resorption after application of a continuous torque moment. *The Angle Orthodontist*, 77(4), 653-659.

Janson G, Sathler R, Fernandes TMF, Branco NCC, de Freitas MR (2013). Correction of Class II malocclusion with Class II elastics: A systematic review. *American Journal of Orthodontics and Dentofacial Orthopedics*, 143(3), 383-392.

Jones G, Buschang PH, Kim KB, Oliver DR (2008). Class II non-extraction patients treated with the forsus fatigue resistant device versus intermaxillary elastics. *The Angle Orthodontist*, 78(2), 332-338.

Knop L, Gandini LG Jr, Shintcovsk RL, Gandini MR (2015). Scientific use of the finite element method in Orthodontics. *Dental Press Journal of Orthodontics*, 20(2), 119-125.

Kucukkurt S (2019). Finite element stress analysis method and researches on dental implantology. *Journal of Dental Faculty of Atatürk University*, 29(4), 701-710.

Li LL, Wang ZY, Bai ZC, Mao Y, Gao B, Xin HT, Zhou B, Zhang Y, Liu B (2006). Three-dimensional finite element analysis of weakened roots restored with different cements in combination with titanium alloy posts. *Chin Med J*, 119(4), 305-311.

Liu DS, Chen YT (2015). Effect of thermoplastic appliance thickness on initial stress distribution in periodontal ligament. *Advances in Mechanical Engineering*, 7(4), 168781401557836.

Liu L, Song Q, Zhou J, Kuang Q, Yan X, Zhang X, Shan Y, Li X, Long H, Lai W (2022). The effects of aligner overtreatment on torque control and intrusion of incisors for anterior retraction with clear aligners: A finite-element study. *American Journal of Orthodontics and Dentofacial Orthopedics*, 162(1), 33-41.

Liu X, Cheng Y, Qin W, Fang S, Wang W, Ma Y, Jin Z (2022). Effects of upper-molar distalization using clear aligners in combination with Class II elastics: a three-dimensional finite element analysis. *BMC Oral Health*, 22(1), 546.

Liu X, Wang W, Gao J, Qin W, Wen Y, Luo H, Ma Y, Jin Z (2023). Actual contribution ratio of maxillary and mandibular molars for total molar relationship correction during maxillary molar sequential distalization using clear aligners with Class II elastics: A finite element analysis. *American Journal of Orthodontics and Dentofacial Orthopedics*, 164(4), e106-e120.

Luzi C, Luzi V (2013). Traitement de la classe II squelettique au moyen d'un appareil de Herbst à ancrage osseux. *L'Orthodontie Française*, 84(4), 307-318.

Nelson B, Hägg U, Hansen K, Bendeus M (2007). A long-term follow-up study of Class II malocclusion correction after treatment with Class II elastics or fixed functional appliances. A*merican Journal of Orthodontics and Dentofacial Orthopedics*, 132(4), 499-503.

Nucera R, Dolci C, Bellocchio AM, Costa S, Barbera S, Rustico L, Farronato M, Militi A (2022), Portelli M. Effects of composite attachments on orthodontic clear aligners therapy: A systematic review. *Materials*, 15(2), 533.

Patterson BD, Foley PF, Ueno H, Mason SA, Schneider PP, Kim KB (2021). Class II malocclusion correction with Invisalign: Is it possible? *American Journal of Orthodontics and Dentofacial Orthopedics*, 159(1), e41-e48.

Rossini G, Parrini S, Castroflorio T, Deregibus A, Debernardi CL (2015). Efficacy of clear aligners in controlling orthodontic tooth movement: A systematic review. *The Angle Orthodontist*, 85(5), 881-889.

Rossini G, Schiaffino M, Parrini S, Sedran A, Deregibus A, Castroflorio T (2020). Upper second molar distalization with clear aligners: A finite element study. *Applied Sciences*, 10(21), 7739.

Staderini E, Ventura V, Meuli S, Maltagliati L, Gallenzi P (2022). Analysis of the changes in occlusal plane inclination in a Class II deep bite "teen" patient treated with clear aligners: A case report. *International Journal of Environmental Research and Public Health*, 19(2), 651.

Tanne K, Sakuda M, Burstone CJ (1987). Three-dimensional finite element analysis for stress in the periodontal tissue by orthodontic forces. *American Journal of Orthodontics and Dentofacial Orthopedics*, 92(6), 499-505.

Turkkahraman H, Eliacik SK, Findik Y (2016). Effects of miniplate anchored and conventional Forsus Fatigue Resistant Devices in the treatment of Class II malocclusion. *The Angle Orthodontist*, 86(6), 1026-1032.

Unal T, Celikoglu M, Candirli C (2015). Evaluation of the effects of skeletal anchoraged Forsus FRD using miniplates inserted on mandibular symphysis: A new approach for the treatment of Class II malocclusion. *The Angle Orthodontist*, 85(3), 413-419.

Wang Q, Dai D, Wang J, Chen Y, Zhang C (2022). Biomechanical analysis of effective mandibular en-masse retraction using Class II elastics with a clear aligner: a finite element study. *Progress in Orthodontics*, 23(1), 23.